Distinguishing Fabry-Perot from guided resonances in thin periodically-textured silicon absorbers

Ahmadpanahi, S.H.; Vismara, R.; Isabella, O.; Zeman, M.

DOI
10.1364/OE.26.00A737

Publication date
2018

Document Version
Final published version

Published in
Optics Express

Research Article | Vol. 26, No. 18 | 3 Sep 2018 | OPTICS EXPRESS A737
Optics EXPRESS

Distinguishing Fabry-Perot from guided resonances in thin periodically-textured silicon absorbers

H. AHMADPANAHI,* R. VISMARA, O. ISABELLA, AND M. ZEMAN

Department of Electrical Sustainable Energy, Delft University of Technology, Delft, the Netherlands
S.H.Ahmadpanahi@tudelft.nl

Abstract: Periodic texturing is one of the main techniques for light-trapping in thin-film solar cells. Periodicity allows for the excitation of guided modes in the structure and, thus, largely enhances absorption. Understanding how much a guided resonance can increase the absorption is therefore of great importance. There is a common method to understand if an absorption peak is due to the excitation of a guided mode, using dispersion diagrams. In such graphs, a resonance is identified as the intersection of a guided-mode-line of a uniform waveguide (with the same optical thickness as the grating structure) with the center of a Brillouin zone of the grating. This method is unfortunately not reliable when the grating height is comparable with the thickness of the wave-guide, or when the thickness of the wave-guide is much larger than the wavelength. In this work, we provide a novel approach to calculate the contribution of a guided resonance to the total absorption in a periodic waveguide, without using the dispersion diagram. In this method, the total electric field in the periodic structure is described by its spatial frequencies, using a Fourier expansion. Fourier coefficients of the electric field were used to calculate the absorption of each diffraction order of the grating. Rigorous numerical calculations are provided to support our theoretical approach. This work paves the way for a deeper understanding of light behavior inside a periodic structure and, consequently, for developing more efficient light-trapping techniques for solar cells applications.

OCIS codes: (050.2230) Fabry-Perot; (310.2790) Guided waves; (050.1950) Diffraction gratings; (070.2575) Fractional Fourier transforms; (260.2110) Electromagnetic optics; (260.5740) Resonance.

References and links

1. A. Reinders, P. Verlinden, W. Sark, and A. Freundlich, *Photovoltaic Solar Energy: From Fundamentals to Applications*, (John Wiley & Sons, Ltd. 2017).
2. C. Schinke, P. C. Peest, J. Schmidt, R. Brendel, K. Bothe, M. R. Vogt, I. Kröger, S. Winter, A. Schirmacher, S. Lim, H. T. Nguyen, and D. MacDonald, "Uncertainty analysis for the coefficient of band-to-band absorption of crystalline silicon," AIP Adv. **5**(6), 067168 (2015).
3. F. J. Haug and C. Ballif, "Light management in thin film silicon solar cells," Energy Environ. Sci. **8**(3), 824–837 (2015).
4. M. Zeman, O. Isabella, S. Solntsev, and K. Jäger, "Modelling of thin-film silicon solar cells," Sol. Energy Mater. Sol. Cells **119**, 94–111 (2013).
5. B. Yan, G. Yue, L. Sivec, J. Yang, S. Guha, and C. Jiang, "Innovative dual function nc-SiOx:H layer leading to a >16% efficient multi-junction thin-film silicon solar cell," Appl. Phys. Lett. **99**(11), 113512 (2011).
6. K. Söderström, G. Bugnon, R. Biron, C. Pahud, F. Meillaud, F. J. Haug, and C. Ballif, "Thin-film silicon triple-junction solar cell with 12.5% stable efficiency on innovative flat light-scattering substrate," J. Appl. Phys. **112**(11), 114503 (2012).
7. T. Matsui, H. Jia, M. Kondo, K. Mizuno, S. Tsuruga, S. Sakai, and Y. Takeuchi, "Application of microcrystalline Si 1- x Ge x infrared absorbers in triple junction solar cells". Photovoltaic Specialists Conference (PVSC), 35th IEEE. 2010; pp 000311– 000316 (2010).
8. J. Bailat, L. Fesquet, J. B. Orhan, Y. Djeridane, B. Wolf, P. Madliger, J. Steinhauser, S. Benagli, D. Borrello, and L. Castens, "Recent developments of high-efficiency micromorph tandem solar cells in KAI-M PECVD reactors," Proc. 25th Eur. Photovoltaic Solar Energy Conf. 5th World Conf. Photovoltaic Energy Convers. pp 2720–2723 (2010).

#327671 https://doi.org/10.1364/OE.26.00A737
Journal © 2018 Received 6 Apr 2018; revised 11 Jun 2018; accepted 15 Jun 2018; published 24 Jul 2018

Optics EXPRESS

9. H. Sakaki, T. Tanoue, K. Yokoyama, D. C. Sun, Y. Sekiguchi, and Y. Yukimoto, "Design and Performances of a Triple (GaAs, Si, and Ge)- Solar-cell System with Multi-layered Spectrum Splitters," Jpn. J. Appl. Phys. **20**(S2), 127 (1981).
10. A. Barnett, D. Kirkpatrick, C. Honsberg, D. Moore, M. Wanlass, K. Emery, and D. Salzman, "Very high efficiency solar cell modules," Prog. Photovolt. Res. Appl. **17**(1), 75–83 (2009).
11. S. Kim, F. Takahashi, S. Kasashima, P. Sichanugrist, T. Kobayashi, T. Nakada, and M. Konagai, "Development of thin-film solar cells using solar spectrum splitting technique", in *proceeding of 38th IEEE Photovoltaic Specialists Conference* (IEEE, 2012), pp 001209–001211.
12. J. Krč, F. Smole, and M. Topič, "Advanced optical design of tandem micromorph silicon solar cells," J. Non-Cryst. Solids **352**(9-20), 1892–1895 (2006).
13. R. Bouffaron, L. Escoubas, V. Brissonneau, J. J. Simon, G. Berginc, P. Torchio, F. Flory, and P. Masclet, "Spherically shaped micro-structured antireflective surfaces," Opt. Express **17**(24), 21590–21597 (2009).
14. M. A. Green, *Solar Cells - Operating Principles, Technology and System Application* (University of NSW: Kensington, Australia, 1992).
15. J. Escarré, K. Söderström, M. Despeisse, S. Nicolay, C. Battaglia, G. Bugnon, L. Ding, F. Meillaud, F. J. Haug, and C. Ballif, "Geometric light trapping for high efficiency thin film silicon solar cells," Sol. Energy Mater. Sol. Cells **98**, 185–190 (2012).
16. S. A. Boden and D. M. Bagnall, "Optimization of moth-eye antireflection schemes for silicon solar cells," Prog. Photovolt. Res. Appl. **18**(3), 195–203 (2010).
17. T. Söderström, F. J. Haug, X. Niquille, and C. Ballif, "TCOs for nip thin film silicon solar cells," Prog. Photovolt. Res. Appl. **17**(3), 165–176 (2009).
18. H. Sai and M. Kondo, "Effect of self-orderly textured back reflectors on light trapping in thin-film microcrystalline silicon solar cells," J. Appl. Phys. **105**(9), 094511 (2009).
19. G. Yue, L. Sivec, J. M. Owens, B. Yan, J. Yang, and S. Guha, "Optimization of back reflector for high efficiency hydrogenated nanocrystalline silicon solar cells," Appl. Phys. Lett. **95**(26), 263501 (2009).
20. K. Söderström, J. Escarré, O. Cubero, F. J. Haug, S. Perregaux, and C. Ballif, "UVnano-imprint lithography technique for the replication of back reflectors for n-i-p thin film silicon solar cells," Prog. Photovolt. Res. Appl. **19**(2), 202–210 (2011).
21. B. Lipovšek, J. Krč, O. Isabella, M. Zeman, and M. Topič, "Modeling and optimization of white paint back reflectors for thin-film silicon solar cells," J. Appl. Phys. **108**(10), 103115 (2010).
22. O. Isabella, S. Dobrovolskiy, G. Kroon, and M. Zeman, "Design and application of dielectric distributed Bragg back reflector in thin-film silicon solar cells," J. Non-Cryst. Solids **358**(17), 2295–2298 (2012).
23. T. Koida, H. Fujiwara, and M. Kondo, "Reduction of Optical Loss in Hydrogenated Amorphous Silicon/Crystalline Silicon Heterojunction Solar Cells by High-Mobility Hydrogen-Doped In 2 O 3 Transparent Conductive Oxide," Appl. Phys. Express **1**, 041501 (2008).
24. C. Das, A. Lambertz, J. Huepkes, W. Reetz, and F. Finger, "A constructive combination of antireflection and intermediate-reflector layers for a-Si / μc-Si thin film solar cells," Appl. Phys. Lett. **92**(5), 053509 (2008).
25. D. Dominé, P. Buehlmann, J. Bailat, A. Billet, A. Feltrin, and C. Ballif, "Optical management in high-efficiency thin-film silicon micromorph solar cells with a silicon oxide based intermediate reflector," Phys. Stat. Sol. **2**(4), 163–165 (2008).
26. S. Faÿ, J. Steinhauser, S. Nicolay, and C. Ballif, "Polycrystalline ZnO: B grown by LPCVD as TCO for thin film silicon solar cells," Thin Solid Films **518**(11), 2961–2966 (2010).
27. H. Iida, N. Shiba, T. Mishuku, H. Karasawa, A. Ito, M. Yamanaka, and Y. Hayashi, "Efficiency of the a-Si:H solar cell and grain size of SnO2 transparent conductive film," IEEE Electron Device Lett. **4**(5), 157–159 (1983).
28. C. Battaglia, C. M. Hsu, K. Söderström, J. Escarré, F. J. Haug, M. Charrière, M. Boccard, M. Despeisse, D. T. Alexander, M. Cantoni, Y. Cui, and C. Ballif, "Light Trapping in Solar Cells: Can Periodic Beat Random," ACS Nano **6**(3), 2790–2797 (2012).
29. O. Isabella, A. Campa, M. Heijna, W. Soppa, R. van Ervan, R. Franken, H. Borg, and M. Zeman, "Diffraction gratings for light trapping in thin-film silicon solar cells," *Conference Record of the 23rd European Photovoltaic Solar Energy Conference*, 2320– 2324 (2008).
30. N. Senoussaoui, M. Krause, J. Müller, E. Bunte, T. Brammer, and H. Stiebig, "Thin-film solar cells with periodic grating coupler," Thin Solid Films **451–452**, 397–401 (2004).
31. C. Haase and H. Stiebig, "Optical properties of thin-film silicon solar cells with grating couplers," Prog. Photovolt. Res. Appl. **14**(7), 629–641 (2006).
32. Z. Yu, A. Raman, and S. Fan, "Fundamental limit of nanophotonic light trapping in solar cells," Proc. Natl. Acad. Sci. U.S.A. **107**(41), 17491–17496 (2010).
33. A. Naqavi, F. J. Haug, C. Battaglia, H. P. Herzig, and C. Ballif, "Light trapping in solar cells at the extreme coupling limit," J. Opt. Soc. Am. B **30**(1), 13–20 (2013).
34. A. Abass and C. Rockstuhl, "Analytical Model of Guided Modes in Structures with Rough Surfaces," in *Light, Energy and the Environment* 2015, OSA Technical Digest (online) (Optical Society of America, 2015), paper PTh2B.3.
35. F. J. Haug, K. Söderström, A. Naqavi, and C. Ballif, MRS Proceedings 1321, 11 (2011).
36. K. Söderström, F. J. Haug, J. Escarré, O. Cubero, and C. Ballif, "Photocurrent increase in n-i-p thin film silicon solar cells by guided mode excitation via grating coupler," Appl. Phys. Lett. **96**(21), 30–32 (2010).

Optics EXPRESS

37. F. J. Hauga, T. Söderström, O. Cubero, V. Terrazzoni-Daudrix, and C. Ballif, "Influence of the ZnO buffer on the guided mode structure in Si/ZnO/Ag multilayers," J. Appl. Phys. **106**, 4 (2009).
38. P. N. Saeta, V. E. Ferry, D. Pacifici, J. N. Munday, and H. A. Atwater, "How much can guided modes enhance absorption in thin solar cells?" Opt. Express **17**(23), 20975–20990 (2009).
39. U. W. Paetzold, S. Lehnen, K. Bittkau, U. Rau, and R. Carius, "Nanoscale observation of waveguide modes enhancing the efficiency of solar cells," Nano Lett. **14**(11), 6599–6605 (2014).
40. K. Söderström, *Coupling light into thin silicon layers for high-efficiency solar cells*, PhD thesis, (STI, Lausanne, 2013).
41. O. Isabella, R. Vismara, D. N. P. Linssen, K. X. Wang, S. Fan, and M. Zeman, "Advanced light trapping scheme in decoupled front and rear textured thin-film silicon solar cells," Sol. Energy **162**, 344–356 (2018).
42. F. J. Haug, K. Söderström, A. Naqavi, and C. Ballif, "Resonances and absorption enhancement in thin film silicon solar cells with periodic interface texture," J. Appl. Phys. **109**(8), 084516 (2011).
43. A. Naqavi, F. J. Haug, C. Ballif, T. Scharf, and H. P. Herzig, "Limit of light coupling strength in solar cells," Appl. Phys. Lett. **102**(13), 131113 (2013).
44. J. Bogdanowicz, *Photomodulated Optical Reflectance: A Fundamental Study Aimed at Non-Destructive Carrier Profiling in Silicon,* (Springer, 2012), p.39–51.
45. R. Bracewell, *The Fourier Transform and Its Applications,* 3rd ed. (McGraw-Hill), p.120.
46. J. Y. Stein, *Digital Signal Processing: A Computer Science Perspective* (Wiley, 2000). p. 115.
47. J. A. Stratton, *Electromagnetic Theory* (John Wiley & Sons, Inc, 2015), p.83–159.

1. Introduction

Semiconductor materials fail to absorb low energy photons efficiently, especially in case of indirect band gap. This means that the quantum efficiency of a semiconductor device drops dramatically close to the materials band gap. In some applications, such as photovoltaics (PV), the absorption of every single photon is important for improving the device conversion efficiency. In materials with a low absorption coefficient near their band-gap, a low-energy photon has to travel a relatively large distance before it is absorbed. Therefore, one can either choose the absorber thickness to be (much) larger than the penetration depth of photons at a specific wavelength, or to deploy light management techniques to increase light capturing. Although increasing the absorber thickness might increase light absorption, it does not necessarily improve the efficiency of corresponding semiconductor devices, since photo-generated charge carriers have to be collected at the contacts. Moreover, in applications like solar cells material cost represents almost 40% of the final cell cost [1]. Additionally, it is very impractical to use thicker layer to absorb, for example, a photon with wavelength 1200 nm using crystalline silicon (c-Si). In that case, an absorber thickness of almost 1 meter would be required [2]. Therefore, it is more practical, economic and efficient to employ light management techniques to absorb a wide range of wavelength using the thinnest possible absorber. Depending on the application, there are many different approaches for light management. In this article, we limit ourselves to light management techniques applied to thin-film hydrogenated nano-crystalline silicon (nc-Si:H) solar cells. This material was chosen because its technology is well developed, its efficiency does not vary much from cell to module, and its indirect band gap makes it a useful test bed for assessing the quality of light management techniques [3]. Light management covers a wide range of techniques that aim to maximize the in-coupling and absorption of solar radiation in the absorber layer [4]. This can be achieved by: (i) efficiently using the solar spectrum, employing multi-junctions [5–8] or spectrum splitters [9–11]; (ii) enhancing light in-coupling by applying anti-reflection (AR) coatings [12–14] or sub-wavelength textures [15,16]; (iii) using low optical loss back reflectors to avoid light dissipation [17–25]; (iv) minimizing absorption is supporting layers [23,26]; (v) promoting light scattering or diffraction by deploying wavelength-scale random [17,18,27] or periodic [28–32] texturing, respectively. Random texturing allows the excitation of all modes in the absorber, whereas periodic texturing gives the possibility to excite discrete resonances such as guided modes. Since most of the energy of a guided mode is confined inside the guiding layer [33] for relatively long distances, guided mode excitation leads to a large enhancement of the absorption. In case of a periodic grating, each diffraction order can excite a resonance in the thin film, which is identified by a peak in the absorption diagram. Therefore, understanding the origin of absorption peaks is instrumental in developing more

effective light trapping techniques [34–39]. In thin films endowed with gratings, the most common method to identify the origin of a resonance is to check, in a dispersion diagram, the crossing point between the wave-guided modes of a flat wave-guide and the centers of Brillouin zones of the grating. Where such an intersection occurs, the excitation of a guided mode is triggered, resulting in a particular absorption peak [39]. In this contribution, such technique is called the intersection method, and presents a number of shortcomings. The dispersion diagram of a waveguide strongly depends on the thickness, material, interface profile, and the surrounding material of the waveguide. Usually, the effective waveguide thickness increases due to the penetration of electromagnetic fields – to a finite extent – into the surrounding media. This influences the accuracy of the dispersion diagram. Moreover, applying texturing leads to distortion of the mode diagram of a flat waveguide. If the grating height is large with respect to the waveguide thickness, the distortion could be significant, and the intersection method cannot predict the guided resonance. The issue is particularly evident for TM polarization [40]. Additionally, if the absorber supports many number of modes in a wide range of wavelengths, as in the case of thin-film solar cells, guided mode lines in the dispersion diagram become very dense. It thus become challenging to trace a guided mode using the intersection method. Finally, if an absorption peak is the result of multiple mode excitations, this method fails to define the contribution of each resonance in total absorption. In this article we provide a different method to overcome the limitations of intersection method and to deliver a deeper understanding of light behavior inside a periodic wave-guide. In this method, Fourier expansion is employed to decompose the electric field inside the absorber and to calculate the contribution of each resonance in enhancing the total absorption in a thin-film, for the entire wavelength range of interest. This article is organized as follows: in section 2, we describe the limitation of the intersection method more explicitly and we define the framework of our new approach. In section 3, we describe the theory used to derive the absorption of each diffraction order. In section 4, we provide the simulation results obtained by applying the theory and eventually in the final section we draw our conclusion.

2. Methodology

Consider a flat 1-μm thick nc-Si:H film, illuminated with TE-polarized light under normal incidence and in the wavelength range between 400 nm and 900 nm (see Fig. 1(a)). In the uniform film of Fig. 1(a), partially reflected light bounces between the two flat interfaces and, in case of constructive interference, a Fabry-Perot (FP) resonance occurs. Absorption in this structure is shown by the green-dashed line in Fig. 1(c). To increase the optical performance, one can apply an AR coating or a sub-wavelength texture to the top surface, to increase light in-coupling, and simultaneously prevent light dissipation by adding a good back reflector at the back side. According to reciprocity principle, increasing light in-coupling raises the chance of light out-coupling as well. The presence of a back reflector strongly enhances absorption, but only for specific wavelengths (where constructive interference occurs). Moreover, based on Snell's law, the angle of refraction inside the structure can never exceed the critical angle (of total internal reflection). Therefore, as long as the system is optically flat and the direction of illumination is perpendicular to the surface, light can never be trapped inside the film. From light management perspective, the motivation for adding the periodicity is to confine the incident energy in the absorber, by exciting the guided modes of a structure such as the one illustrated in Fig. 1(b). Both flat and textured structures are surrounded by air and are made of nc-Si:H. The textured structure has the same physical thickness as the flat film, and it is illuminated under the same conditions. The optimized grating period for thin-film applications is usually defined by the material band-gap [41], which is around 1100 nm for nc-Si:H. In this work, we aim to track different guided modes and study their contribution to total absorption. To make our model as simple as possible, we avoid exciting an excessive amount of modes by choosing a grating period of 600 nm. Additionally, to study the evolution of guided modes with respect to FP resonances, we want to avoid disturbing the

Optics EXPRESS

guided modes of the flat structure. Thus, a shallow grating with a height of only 20 nm was initially chosen. Later, investigation of taller structures (300 nm) will be also carried out. The duty cycle (dc) of the grating is fixed to 0.5. The absorption in the shallow grating structure is shown by the solid-red line in Fig. 1(c) and exhibits a clear enhancement with respect to the flat structure. Intuitively, two different types of peaks can be recognized in this curve: the first is very similar to the peaks in the green-dashed curve (flat case). These peaks, indicated by blue arrows, are associated with FP resonances in the grating structure, because their peak positions are the same as the ones of FP resonances in the flat structure. The second types of peaks are sharp and narrow, occurring where there is low absorption in the green-dashed curve. These peaks are most probably the result of the excitation of guided modes via the grating. This hypothesis can be verified using the intersection method. Figure 2(a) shows the dispersion diagram of the flat structure in Fig. 1. Figure caption (a), in the wavelength range between 700 nm and 850 nm. Open circles indicate the intersection of a guided mode (blue line) and the center of one Brillouin zone (grey horizontal lines). The wavelength of each intersection in Fig. 2(a) corresponds with absorption peaks in Fig. 2(b).

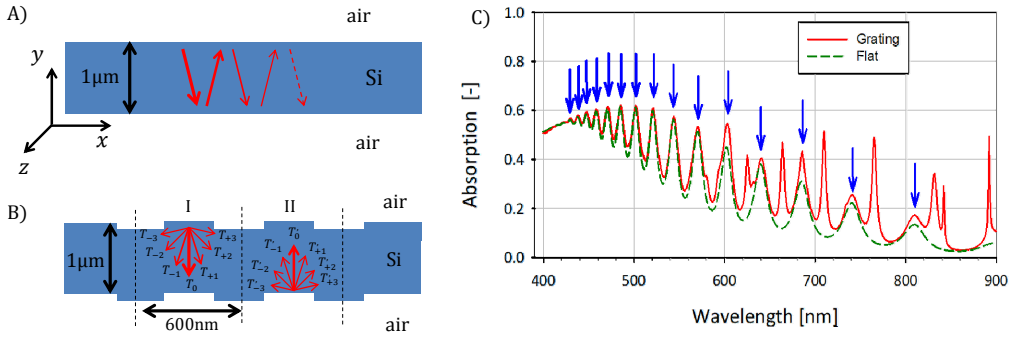

Fig. 1. A) A 1-μm thick nc-Si:H film and partial reflection of light inside the structure. B) A nc-Si:H waveguide, endowed with conformal gratings and characterized by a total thickness of 1 μm at every point. Region I and II show light scattering from each interface. T_i and T'_i are the transmission and reflection from the top and bottom interfaces, respectively. C) Absorption in the flat film (dashed–green line), and in the grating structure (red line). Blue arrows indicate FP resonance peaks.

It is apparent that this method can, to some extent, confirm that a particular absorption peak is matched with one of the grating orders. However, it does not provide any information about the relative weight of an excited mode in total absorption coupling [42]. This is important because, in a grating structure such as the one of Fig. 1(b), the field scatters into many discrete angles after passing through the first interface. T_i and T'_i are the transmission and reflection from the top and bottom interfaces, respectively. The region which is marked by I shows scattering from the first interface. Scattered field from top surface (T_i in region I) travels through the film and reaches the second interface. Due to the periodicity of the bottom surface, each diffraction order of top surface can further diffract into all available diffraction orders (T'_i in region II). For example, T_{+2} from the top interface can produce all T_i' orders when it reaches the second interface. This multiple scattering allows the energy to couple from one mode to another, creating an absorption peak which is the result of multiple mode excitations. If the height of grating is small (with respect to the wave-guide thickness), the presence of the grating can be seen as a small perturbation in the refractive index or in the geometry of the wave-guide [43]. This means that the dispersion diagram of the perturbed wave-guide is very similar to the one of flat wave-guide. If the grating height is large, the dispersion diagram of the grating wave guide might differ significantly from the one of flat structure, and the *intersection method* does not provide reliable result. All these suggest that a different method or tool is needed to enable the analysis of thin-film structures endowed with

Optics EXPRESS

grating. This can help to have a better understanding of light trapping and absorption in the area of thin-film solar cells.

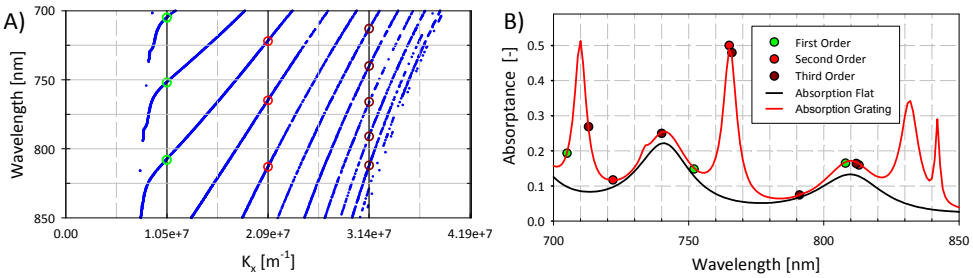

Fig. 2. A) Dispersion diagram of the flat structure. Vertical axes show the wavelength of light and horizontal axis represents the order of Brillouin zones and the corresponding value of k_x. Blue lines show the position of guided modes in the flat structure, while the open circles indicate where they intersect with the centers of Brillouin zones. B) Absorptance spectra between 700 nm and 850 nm. Circles on the grating absorption (red) curve correspond to intersections between the centers of Brillouin zones of the grating and a guided mode of the flat structure in (A).

3. Theoretical background

Absorption in a dielectric with volume V is proportional to the integral of the squared magnitude of the electric field over the volume of the material. Since we are modelling a 1-D grating, the integral over a surface S can be considered:

$$A = \varepsilon_0 n \kappa \omega \int_S \left| E(x,y) \right|^2 dxdy \tag{1}$$

where n and κ are real and imaginary parts of the refractive index, respectively, ε_0 is the dielectric constant of vacuum, and ω is the angular frequency. The grating vector (periodicity) is along the x direction, while the y axis is along the thickness of the film (see Fig. 3(a)). Since the structure is periodic, the electric field inside the film can be expanded using a Fourier expansion [44,45]. Generally, this can be done by diving the grating structure into many small sub-layers along the y direction (horizontal lines marked with Y_i in Fig. 3(a)). For shallow gratings, we only consider the uniform part of the structure (light blue region in Fig. 3(a)). For large grating structures, however, the top and bottom grating rims are also taken into account. The structure (large grating) is divided into top, middle and bottom parts. Top and bottom parts are shown in dark blue color in Fig. 3(a), and middle part is shown in light blue color. Each part is then divided into many thin sub-layers. The number of sub-layers is defined such that for the shortest wavelength-in-material ($\lambda = \lambda_0/n$) within the spectral range of interest, there are at least five sub-layers along one wavelength. In this way, for each wavelength there are at least 5 sampling points in the material. For each wavelength and polarization, the electric field can be then described as:

$$\boldsymbol{E}(\boldsymbol{x},\boldsymbol{y},\boldsymbol{\lambda}_0,\boldsymbol{\theta}_i) = \sum_{\boldsymbol{i}=\boldsymbol{y}_1}^{\boldsymbol{i}=\boldsymbol{y}_n} \sum_{\boldsymbol{q}=-\infty}^{\boldsymbol{q}=+\infty} \boldsymbol{c}_{i,q,\lambda_0,\theta_i} \, \boldsymbol{e}^{\,j\left(\frac{2\pi}{\lambda_0}\sin(\theta_i)\pm q\frac{2\pi}{\Lambda}\right)x} \tag{2}$$

where $j = \sqrt{-1}$, q and Λ are grating order and periodicity, respectively, $c_{(i,q,\lambda_0,\theta_i)}$ is q^{th} Fourier coefficient of the electric field with wavelength λ_0 in the i^{th} sub-layer for the incidence angle equal to θ_i. Total Fig. 3(b) shows the TE polarized electric field profile for the 60th sub-layer at 400 nm. Multiplying Eq. (2) by its complex conjugate and integrating over one period (i.e. applying Parseval's theorem), we arrive to the energy of the electric field in one sub-layer

Optics EXPRESS

[46,47]. Figure 3(c) illustrates the energy spectrum of the electric field up to 10 orders, for λ_0 = 400 nm in the 60th sub-layer. In other words, such diagram exactly shows how the total energy in the 60th sub-layer is distributed within different diffraction orders of grating.

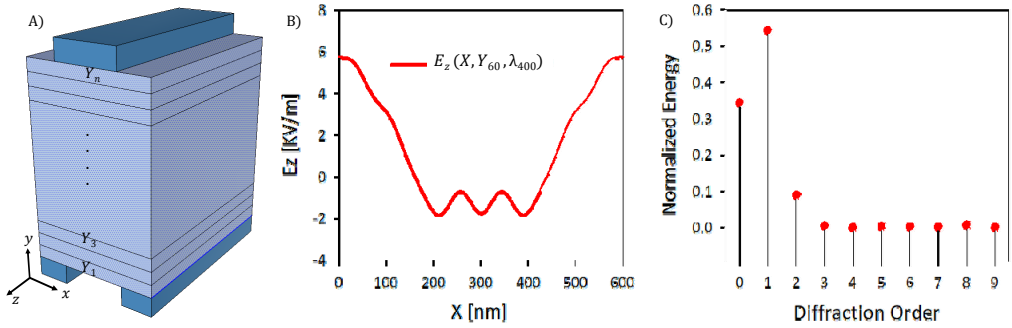

Fig. 3. A) One period of the grating structure. The light blue region is the uniform part of the film, which is divided into *i* thin sub-layers, each with thickness Y_i. B) Intensity of the TE-polarized electric field in the 60th sub-layer, at λ_0 = 400 nm. C) First 10 orders of energy spectral density for the electric field, in sub-layer 60 at λ_0 = 400 nm. The energy is normalized by the total energy in one sub-layer.

The symmetry of the electric field implies a symmetry in energy distribution, that is $T_{-i} = T_{+i}$. Therefore, the total energy in T_i is actually equal to $T_{-i} + T_{+i}$. For example, in Fig. 3(c), the first diffraction order contains 55% of the total energy, meaning that $T_{-1} = T_{+1} = 27.5\%$ of the total energy. Summing the energy of all sub-layers, we end up with the total electric energy stored in one period of the grating (Λ):

$$\int_0^y \int_0^\Lambda \left|E\left(x,\lambda_0,\theta_i\right)\right|^2 dxdy = \sum_{i=y_1}^{i=y_n} \sum_{q=-\infty}^{q=+\infty} \int_0^\Lambda \left|c_{i,q,\lambda_0,\theta_i}\right|^2 dx \tag{3}$$

the left-hand side of Eq. (3) represents the total electric energy in one period, while the right-hand side of this equation describes the distribution of energy per each diffraction order in one period. Multiplying both sides of Eq. (3) by $\varepsilon_0 n k \omega$ yields:

$$\varepsilon_0 nk\omega \int_0^y \int_0^\Lambda \left|E\left(x,\lambda_0,\theta_i\right)\right|^2 dxdy = \varepsilon_0 nk\omega \sum_{i=y_1}^{i=y_n} \sum_{q=-\infty}^{q=+\infty} \int_0^\Lambda \left|c_{i,q,\lambda_0,\theta_i}\right|^2 dx \tag{4}$$

where the left-hand side is the total absorption, while the right-hand side represents the total absorption in terms of diffraction orders. $\left|c_{(i,q,\lambda_0,\theta_i)}\right|^2$ is a function of θ_i, which implies that each Fourier component of electric field varies based on the incidence angle. Therefore, for each incidence angle, Eq. (4) needs to be applied. In this work, θ_i is considered to be zero and thus further on we omit the sub-index of θ_i. The electric file inside the absorber is the input for Eq. (4). This means that the electric field distribution inside the absorber has to be calculated separately using a rigorous electromagnetic simulation tool at optical frequencies. This rigorously calculated electric filed then is used to calculate the Fourier coefficients.

4. Results and discussion

Equation (4) is used to study the absorption pattern of the structure of Fig. 1(b), with two different grating heights: 20 nm (shallow structure, H20) and 300 nm height (large structure, H300). COMSOL Multiphysics was employed, to rigorously calculate the electric field inside these architectures. Both structures are excited under normal incidence, and the absorption is calculated (for TM and TE polarization) in the wavelength range 400 nm – 1100 nm. For each wavelength, the calculation is done according to the real and imaginary parts of nc-Si:H

refractive index at corresponding wavelength. We use Red lines in Fig. 4(a) to Fig. 4(d) display absorption values directly computed by COMSOL in one period of the model. For λ_0 > 460 nm, the absorption coefficient of nc-Si:H decreases, hence the incident radiation can penetrate deeper into the film.

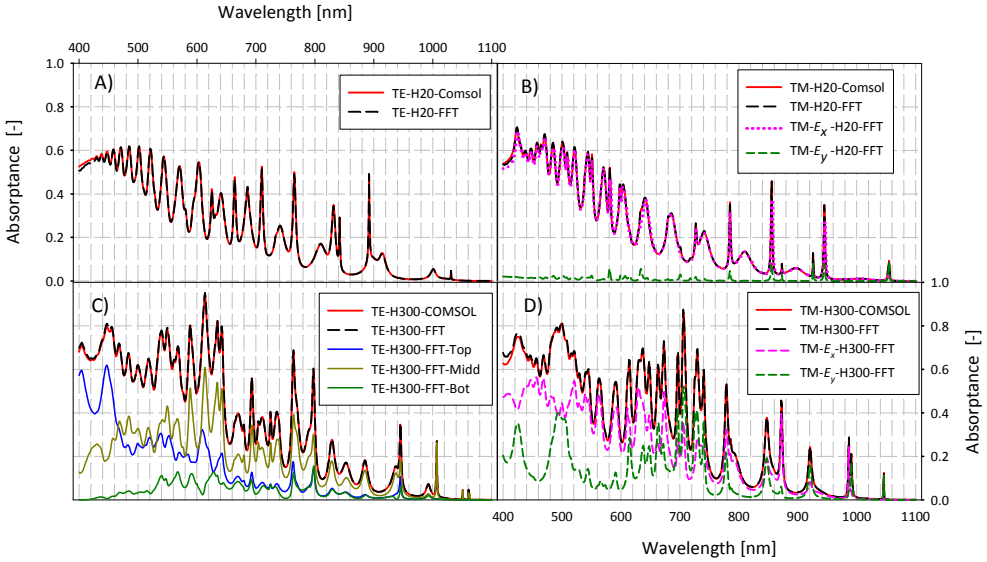

Fig. 4. A) absorption for TE-polarized light and B) absorption for E_x and E_y components of TM-polarized light, in the shallow structure. Red lines represent light absorption calculated directly by COMSOL, while black lines show light absorption in the uniform part of the model. C) and D) represent light absorption - in the architecture endowed with large gratings - for TE and TM polarizations, respectively. Solid–red and dashed–black lines show the total absorption calculated by COMSOL and Eq. (4), respectively. Blue, grey and green colored curves in C) represent absorption in the top, middle, and bottom parts of the large structure (see Fig. 3(a)), for TE-polarized light. Dashed pink and green colored curves in D) show absorption in the large structure for E_x and E_y components of TM-polarized light, respectively.

For this reason, it is mostly absorbed in the middle part of the structure. Absorption in large grating structure for TM polarized light is presented in Fig. 4(d). The small difference between computed (by COMSOL) and calculated (with Eq. (4) absorption – for λ_0 < 420 nm – can be attributed to meshing in COMSOL. In fact, the TM-polarized electric field is discontinuous at the nc-Si:H / air interface, hence great variation of the field in that area can be expected. This is not the case for TE-polarized light, hence such difference is not observed in Fig. 4(c). Nevertheless, for solar cell applications the main focus is on longer wavelengths, for which the absorption calculated by Eq. (4) very well matches with the rigorous calculation done by COMSOL. It can be observed that the absorption by the E_y component of the TM-polarized electric field is much stronger in the large structure, with respect to the shallow structure (Fig. 4(b)). This indicates that the energy content in higher diffraction orders is greater for tall grating than for shallow ones. The reason is explicitly discussed in the section "TM polarization."

4.1 TE polarization (E_z component)

Figure 5(a) illustrates one period of the grating structure as well as the orientation of the incident and transmitted electric field outside and inside this structure, respectively. Inside the absorber in Fig. 5(a), one can see the direction of oscillation and propagation of one of the diffracted plane waves inside the absorber (in time domain), before it reaches the bottom surface. Total field inside the structure is the sum of transmitted field from top interface and scattered field from the second interface. For TE polarization, the electric field of the incident

Optics EXPRESS

wave is perpendicular to the plane of incidence and the electro-magnetic field propagates along y direction.

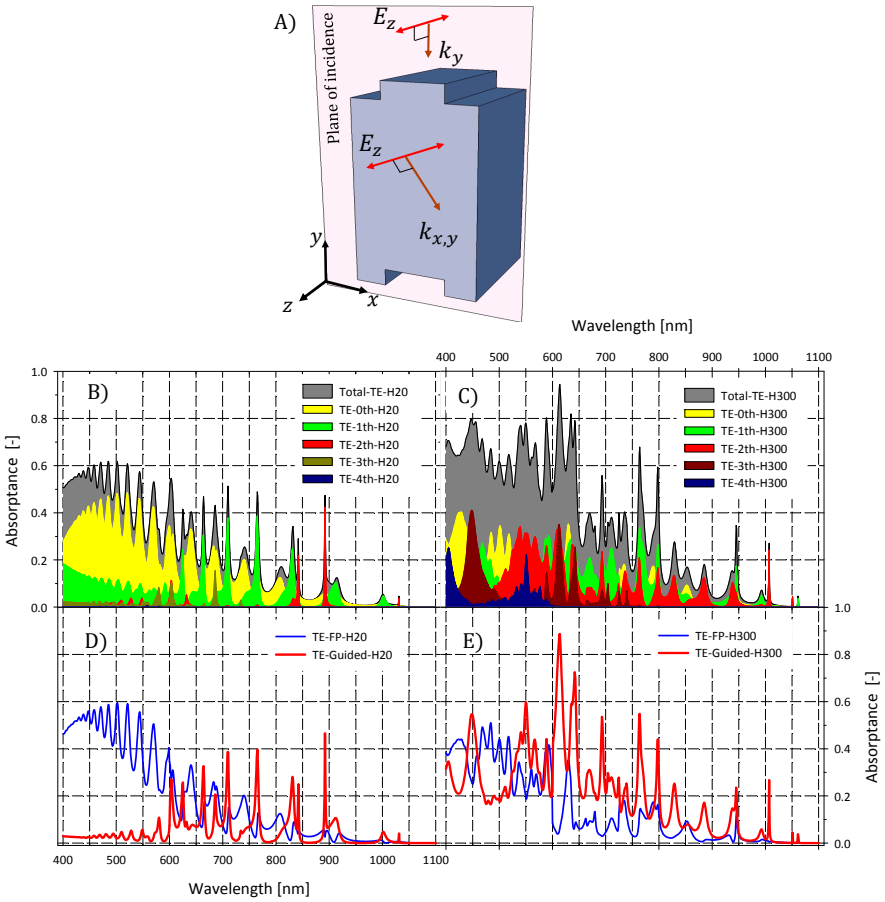

Fig. 5. A) orientation of incident and transmitted electric field for one period of the grating structure for TE polarization. B) Each color indicates the total absorption for different diffraction order in the uniform part of the shallow grating structure. C) Absorption by each diffraction order in large grating structure is represented by different colors. Total absorption for TE polarization is shown in grey. D) and E) present total FP (blue lines) and guided resonance (red lines) triggered by the absorption of TE polarized light, for *shallow* and *large structure* respectively.

The transmitted field has its electric field along z direction, but its wave vector gains x component and falls in the (x, y) plane. Figure 5(b) presents the total absorption in the uniform part of the shallow structure when it is excited by TE polarized light. Each color in the graph represents the total absorption by one of the gratings order. As it has been addressed before, the shallow grating is not able to diffract the incident energy efficiently. This means that the incident field is not perturbed much by the grating structure and most of the incident energy does not *feel* the grating. This is the reason why the zeroth diffraction order (yellow) has the largest contribution in total absorption in Fig. 5(b). It is important to notice that not all the diffraction orders could excite a guided mode resonance. The diffraction angle for each grating order is given by $\beta_m = \sin^{-1}\left(\frac{\sin(\theta_i)}{n} \pm \frac{m \cdot \lambda_0}{n \cdot \Lambda}\right)$, where m is the diffraction order, n is the refractive index, Λ is grating period, λ_0 is the wavelength and θ_i is the angle of incidence. The diffraction angle decreases as the incident wavelength decreases. A diffraction order could

Optics EXPRESS

excite a guided mode resonance only if its diffraction angle is larger than material's critical angle at that wavelength. Therefore, depending on the wavelength, one diffraction order can contribute to FP and guided resonance. For the grating structure in Fig. 1(b) for wavelengths shorter than 600 nm, the first diffraction order contributes to FP resonances because its angle of diffraction is smaller than the critical angle of nc-Si:H in this wavelength range. Therefore, the sharp absorption peaks in green color in Fig. 5(b) are due to the excitation of guided modes via the first diffraction order only for wavelengths longer than 600 nm. Diffraction angle for higher diffraction orders ($m \geq 2$) is larger than critical angle for entire wavelength range of our interest. The zeroth diffraction order ($\beta_0 = 0$) is always a FP resonance. When the grating height is increased, incidence energy could better "feel" the grating. As a result, light absorption corresponded to zero diffraction order decreases significantly and large amount of incidence energy diffracted to higher orders. This can be observed in Fig. 5(c), where the absorption by the zeroth order is not more significant than higher orders for $\lambda < 700$ nm. For longer wavelengths, first and second orders have larger shares in total absorption. According to the gratings equation, the diffraction angle of a grating does not depend on the grating height. Thus, even for large grating structure, the first diffraction order counts as FP resonance for wavelength shorter than 600 nm. In Fig. 5(d) and E, total absorption is distinguished by its resonance type. Blue lines represent the absorption by FP resonance in shallow and large grating structures, respectively. Interestingly, FP absorption is smaller in *large structure* than in *shallow structure*. Instead, absorption triggered by guided mode in *large structure* (red lines) is obviously higher than in *shallow structure*. As we mentioned before, *large structure* diffracts the incident energy more efficient.

4.2 TM polarization

Inside the grating structure, the electric field of TM-polarized light can be described as the superposition of two orthogonally oscillating electric fields, E_x and E_y. The E_x component represents a plane wave propagating along the ± y direction. When the diffraction angle is smaller than the critical angle, the components of electric filed can be seen as a FP resonance, created by partially reflected energy from top and bottom interfaces.

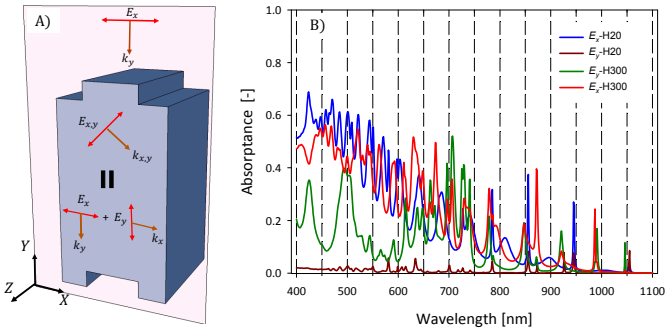

Fig. 6. A) Grating structure and orientation of the electric field before and after reaching the top interface, for TM-polarized illumination. The electric field vector inside the film can be decomposed in to two orthogonally oscillating electric fields, along the *x* and *y*. B) Total absorption by both components of the TM-polarized electric filed, for large and shallow grating structures.

The E_y component, on the other hand, represents a plane wave propagating along the ± x direction (parallel to the grating vector). The Pointing vector inside the waveguide is defined as $\vec{S} = \vec{E} \times \vec{H}$, and represents the direction of propagation of electromagnetic energy [46]. For TM polarization, the magnetic field oscillates along the z axis, thus:

$$\overline{S_m} = S_{x,m} \cdot \hat{x} + S_{y,m} \cdot \hat{y} = \pm E_{y,m} \cdot H_{z,m} \hat{x} \mp E_{x,m} \cdot H_{z,m} \cdot \hat{y} \quad (5)$$

Optics EXPRESS

where the sub index m is the diffraction order, while $\hat{x}$ and $\hat{y}$ are unit vectors in the x and y directions, respectively. Equation (5) shows that, for a particular diffraction order, a larger value of E_y leads to a larger energy flux in the x direction. In addition, in a plane wave the electric field and propagation vectors are always perpendicular to each other. This means that the zeroth diffraction order (with propagating vector along y) has $E_y = 0$. The E_x and E_y components contributes differently in total absorption. In Fig. 6(b) the total absorption due to each components of TM polarized light for shallow and large gratings are shown. We would like to emphasize that the only difference between *large* and *shallow structure* is their grating height. Therefore, any difference in their absorption patterns is directly linked to the different grating height. For example, in Fig. 6(b) a significant increase in absorption of the E_y component in the *large structure* is observed, while E_x absorption does not change dramatically for shallow and large structures.

4.2.1 TM polarization (E_x component)

We first study the light absorption by the x component of the electric field, in the *large* and *shallow structure*. Figure 7 illustrates the absorption of the E_x component of the TM-polarized electric field by each diffraction order, in structures endowed with shallow and large gratings, calculated using Eq. (4) .

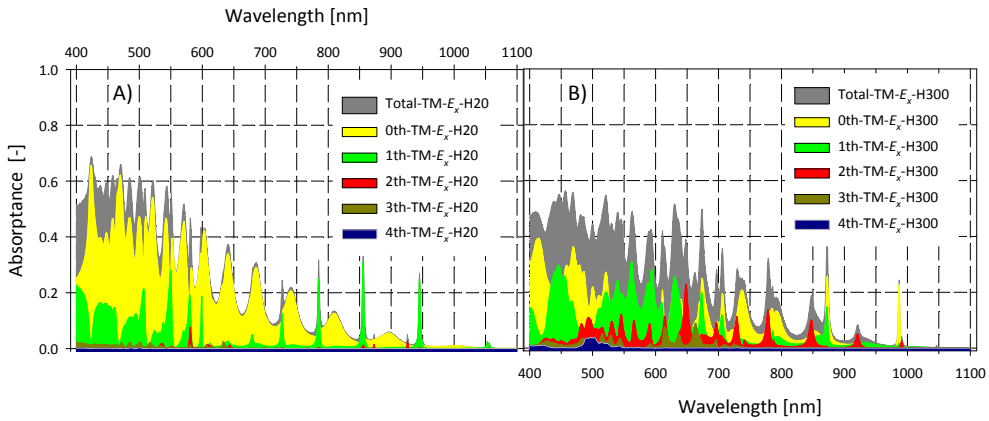

Fig. 7. Total absorption of the Ex component for each diffraction order: inside the uniform part of the shallow grating structure (A), and inside the entire large grating structure (B), for TM-polarized illumination.

For $\lambda_0 < 600$ nm, the correlation between the peaks of the 0th diffraction order and the notches in the 1st diffraction order (Fig. 7 (a)) indicates a strong light coupling between these two orders. In this wavelength range, the diffraction angle of the 1st order is smaller than the critical angle of nc-Si:H, thus first and zero diffraction orders can be considered as FP resonance. For the *shallow structure* it is clear that the contribution of the 0th diffraction order to the total absorption is very large, even at longer wavelengths. This situation indicates FP resonances due to (i) the already addressed low efficiency of the grating and (ii) the propagation vector aligned to the y axis. For $\lambda_0 > 700$ nm, the absorption peaks by the 1st diffraction order can be considered as guided resonance, since in this range the diffraction angle of the 1st order is larger than the critical angle. In the *large structure*, absorption by higher diffraction orders is highly enhanced, while zeroth order triggered absorption is clearly lower (Fig. 7(b)). This implies that larger gratings interact more strongly with the incident radiation, thus diffracting more energy into higher orders.

Optics EXPRESS

4.2.2 TM polarization (E_y component)

Absorption by each diffraction order for the E_y component of the TM-polarized electric field for the *shallow* and *large structure*, calculated with Eq. (4), is presented in Fig. 8(a) and Fig. 8(b), respectively. In section "TM polarization", it was discussed that the E_y component has no 0th diffraction order. In Fig. 8 one can clearly see that the absorption by the 0th diffraction order is zero. All of the absorption peaks in Fig. 8 with $\lambda_0 > 600$ nm are directly connected to the excitation of guided modes, because their diffraction angles are larger than the critical angle. It is important to clarify that for $\lambda_0 < 500$ nm, the sum of absorption by the first 4 diffraction orders of E_y does not yield the total absorption, since orders greater than 4 were not included, because – at short wavelengths – resonance peaks start overlap and cover each other, becoming indistinguishable. This creates an overall flat absorption profile, which does not give much information about the behavior of light inside the structure.

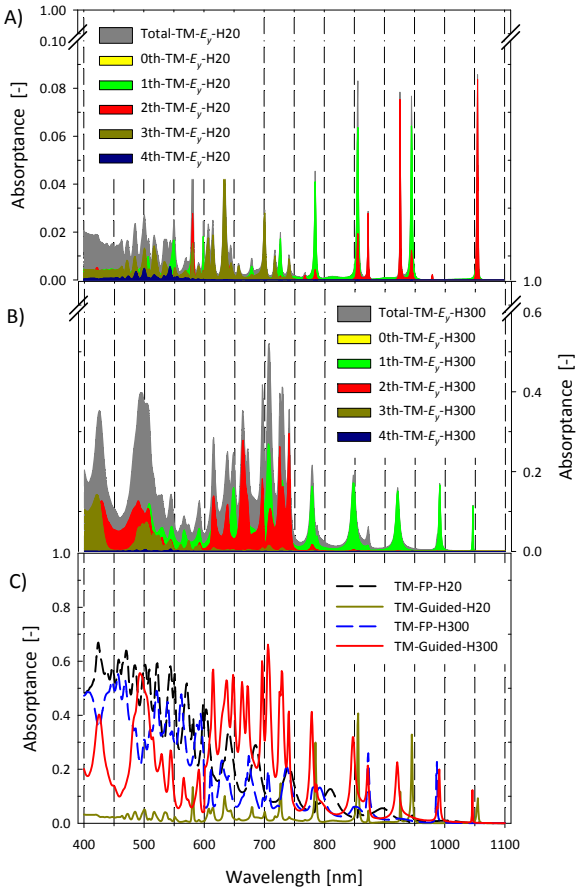

Fig. 8. (A)–(B) Contribution of each diffraction order, for the E_y component of the electric field, to total absorption. (C) Total FP (dashed lines) and guided resonance (continuous lines) triggered absorption, for *shallow* and *large structure*.

Finally, total absorption by TM polarization in the shallow and large structure is decomposed into FP and guided resonance absorption (Fig. 8(c)). Blue and black dashed lines represent total FP absorption in structures with large and shallow gratings, respectively. Going from shallow to large grating, FP absorption is unaffected (for TM-polarized light). However, absorption triggered by guided resonances (solid lines in Fig. 8(c)) are dramatically higher for the large structure, especially $\lambda_0 > 600$ nm. The sudden jump in guided resonance

Optics EXPRESS

absorption at λ_0 = 600 nm is attributed to the contribution of 1st diffraction order to guided resonance.

5. Conclusions

We have provided a different approach to calculate the contribution of different resonances to total absorption, without using a dispersion diagram. In this approach, Fourier expansion is employed to calculate the energy spectral density of the electric field inside a textured structure. This approach is supported by numerical and rigorous calculations, using a software based on the finite element method. We were able to track the origin of each absorption peak, (guided resonance or FP). Using our technique, we were also able to define accurately the relative weight of each resonance in total absorption, for every point in the wavelength range of interest. This method can be used for a large wavelength range and it is not limited by film thickness or grating profile. This approach is also not limited to solar cell applications and can be used to understand the light behavior in any multilayer structure with periodic texturing.